Geophysical Research Letters

RESEARCH LETTER
10.1029/2019GL082015

Anthropogenic Aerosols, Greenhouse Gases, and the Uptake, Transport, and Storage of Excess Heat in the Climate System

D. B. Irving[1], **S. Wijffels**[1,2], **and J. A. Church**[3]

[1]CSIRO Oceans and Atmosphere, Hobart, Tasmania, Australia, [2]Woods Hole Oceanographic Institution, Woods Hole, MA, USA, [3]Climate Change Research Centre, University of New South Wales, Sydney, New South Wales, Australia

Key Points:
- Single forcing simulations suggest anthropogenic aerosols have caused most historical excess heat uptake to occur in the Southern Hemisphere
- This interhemispheric asymmetry in heat uptake is eliminated by a northward oceanic transport of excess heat
- In the future, the storage of excess heat will be skewed toward the Northern Hemisphere

Supporting Information:
- Supporting Information S1
- Text S1

Correspondence to:
D. Irving,
irving.damien@gmail.com

Citation:
Irving, D. B., Wijffels, S., & Church, J. A. (2019). Anthropogenic aerosols, greenhouse gases, and the uptake, transport, and storage of excess heat in the climate system. *Geophysical Research Letters*, *46*, 4894–4903. https://doi.org/10.1029/2019GL082015

Received 10 JAN 2019
Accepted 20 APR 2019
Accepted article online 25 APR 2019
Published online 15 MAY 2019

Abstract The largest contributor to the planetary energy imbalance is well-mixed greenhouse gases (GHGs), which are partially offset by poorly mixed (and thus northern midlatitude dominated) anthropogenic aerosols (AAs). To isolate the effects of GHGs and AAs, we analyze data from the CMIP5 historical (i.e., all natural and anthropogenic forcing) and single forcing (GHG-only and AA-only) experiments. Over the duration of the historical experiment (1861–2005) excess heat uptake at the top of the atmosphere and ocean surface occurs almost exclusively in the Southern Hemisphere, with AAs canceling the influence of GHGs in the Northern Hemisphere. This interhemispheric asymmetry in surface heat uptake is eliminated by a northward oceanic transport of excess heat, as there is little hemispheric difference in historical ocean heat storage after accounting for ocean volume. Data from the 1pctCO2 and RCP 8.5 experiments suggests that the future storage of excess heat will be skewed toward the Northern Hemisphere oceans.

Plain Language Summary Climate change is fundamentally an energy balance problem. Due to the influence of greenhouse gas (GHG) emissions, the amount of solar energy absorbed by Earth is currently greater than the amount of energy radiated to space. This energy imbalance is partially offset by particulate matter released into the atmosphere from burning fossil fuels (anthropogenic aerosols, AAs), which is most concentrated in the northern midlatitudes. In this study, model simulations of the historical and future climate are compared to single forcing simulations that apply only GHG or AA emissions. We find that the historical uptake of excess heat is strongly skewed toward the Southern Hemisphere because AAs cancel the influence of GHGs in the Northern Hemisphere. The oceanic storage of that heat shows little difference between the hemispheres due to a strong northward transport of excess heat. In future, the models suggest excess heat storage will skew toward the Northern Hemisphere.

1. Introduction

Human activities have substantially altered the radiative properties of the atmosphere, giving rise to a planetary energy imbalance (von Schuckmann et al., 2016). The largest contributor to this imbalance is greenhouse gases (GHGs), which are partially offset by anthropogenic aerosols (AAs). In estimates and interpretations of the planetary energy imbalance, the largest source of uncertainty is the magnitude of the AA contribution (−1.9 to −0.1 W/m^2 over the period 1750–2011). By comparison, the GHG contribution is relatively well constrained (2.6 to 3.2 W/m^2; Boucher et al., 2013). Much of the spatial variability in anthropogenic forcing also comes from AAs, because unlike well-mixed GHGs they have mixing timescales that are much longer than their atmospheric residence time (Roelofs, 2013). This means AA concentrations tend to peak near their primary emission sources in the Northern Hemisphere (NH) midlatitudes. These spatial differences between GHG and AA forcing have important implications for how the global top of the atmosphere (TOA) energy imbalance is distributed throughout the climate system. Over 90% of the excess energy is ultimately absorbed by the ocean (von Schuckmann et al., 2016), but how it gets there (via radiative fluxes and atmospheric transport) and where it ends up (via ocean transport) influences the regional characteristics of climate change.

Our current understanding of the uptake, transport, and storage of excess heat associated with anthropogenic forcing is largely derived from state-of-the-art climate models. While observations of the planetary

energy imbalance are improving, the imbalance is small compared to the uncertainties associated with estimates of the overall energy budget, particularly at sub-global scales (von Schuckmann et al., 2016). Single forcing model experiments, such as those conducted as part of Coupled Model Intercomparison Project Phase 5 (CMIP5; Taylor et al., 2012), are also required to understand the separate influence of GHGs and AAs. Studies in this area have focused on a variety of spatial scales, time periods, model experiments, and aspects of the excess energy pathway. For instance, in a recent hemispheric-scale analysis, excess heat uptake at the TOA and ocean surface was shown to be equally distributed between the two hemispheres for the CMIP5 experiment where estimated historical GHG emissions are the only external forcing applied (the "GHG-only" experiment). In contrast, the all-forcing "historical" experiment (which includes AAs) shows a strong interhemispheric asymmetry, with most heat uptake occurring in the Southern Hemisphere (SH; Lembo et al., 2019). Both experiments showed a similar change in ocean heat content (OHC) across the two hemispheres, which implies a northward ocean transport of excess heat in the historical experiment, attributable to AAs.

Instead of using the difference between the historical and GHG-only experiments to infer the influence of AAs, it is possible to directly analyze their influence using data from the "AA-only" single forcing experiment. For instance, analysis of ocean surface heat flux data from the GHG-only and AA-only experiments has shown that much of the historical discrepancy in surface heat uptake between the Southern Ocean (which dominates) and North Atlantic is due to AAs (Shi et al., 2018). Comparisons between the GHG-only and AA-only experiments have actually considered far more than just the energy budget, with many spatial symmetries (Xie et al., 2013) and asymmetries (Wang et al., 2016) identified between GHG and AA forcing for atmospheric and surface variables such as temperature and precipitation. While such analysis of CMIP5 experiments spanning the historical period (1861–2005) has provided valuable insights into the role of anthropogenic forcing in past climatic changes, those insights are not necessarily applicable to the future climate. For instance, AA emissions peaked in the late 20th century and are projected to decline throughout the 21st century (Smith et al., 2016). This likely explains why surface heat uptake is much more evenly distributed between the Southern Ocean and North Atlantic in simulations of the future climate (Shi et al., 2018). Insights into the influence of GHG forcing on the meridional transport of excess heat have also been gained by analyzing CMIP5 experiments that apply much larger GHG increases than have occurred over the historical period (e.g., Huang & Zhang, 2014).

Building on this array of previous studies, we present a comprehensive account of the uptake, transport, and storage of excess heat over the historical period. This includes the TOA, ocean surface, and ocean interior (and transports in between) for both hemispheric and zonally integrated quantities. Results for the historical, GHG-only, and AA-only CMIP5 experiments are presented, with relevant comparisons made to simulations associated with larger GHG increases. In some places our analysis serves to draw together, synthesize, and confirm results from previous studies, while in others new insights are offered.

2. Methods

2.1. Data

The primary CMIP5 experiments used in our analysis were the historical (all anthropogenic and natural forcing), historicalGHG (GHG-only), and historicalAA (AA-only). As part of the collection of historicalMisc (historical miscellaneous) experiments, historicalAA was a lower priority for CMIP5 modeling groups (Taylor et al., 2012) with only 10 models performing the experiment. Six of these models archived the variables required for our analysis (Table S1 in the supporting information). A historicalnoAA (all forcings except AAs) experiment was also included in the historicalMisc collection; however, only two modeling groups ran that experiment, and hence, it was not analyzed here.

In addition to these simulations of the historical climate, we analyzed data from the 1pctCO2 (over a common 140-year period; nominally 1861–2000) and Representative Concentration Pathway 8.5 (RCP 8.5; 2006–2100) experiments. Carbon dioxide concentrations increase at a rate of 1%/year in the 1pctCO2 experiment (i.e., a much faster rate than for the GHG-only experiment), while RCP 8.5 is a "business as usual" (i.e., GHG emissions continue to rise) continuation of the historical experiment (van Vuuren et al., 2011). The piControl (preindustrial control) experiment was also used for the purpose of drift removal (see below). The original time resolution of all data was monthly, from which an annual mean timeseries was calculated before any analysis was conducted.

2.2. Computation

The primary software used to generate the results was Iris (Met Office, 2010–2018). This package builds upon the core Python libraries for handling numerical arrays and plotting—Numpy (Van Der Walt et al., 2011) and Matplotlib (Hunter, 2007)—to greatly simplify data analysis and visualization for atmosphere and ocean scientists. The Seaborn library (Waskom, 2018) was also used to improve the esthetics of the figures.

Following established best practices for reproducibility (Irving, 2016), an accompanying figshare repository has been created to document the computational methodology in more detail (Irving, 2019). It includes a more precise description of the software environment (i.e., software version numbers and dependencies), a copy of the (version controlled) code written to perform the analysis, and details of the data processing steps involved in producing each figure in the paper. A listing of each CMIP5 data file used in this study along with its version number, tracking ID, and data set ID (where available) has also been archived in that repository.

2.3. Heat Uptake

The net TOA radiation (netTOA) was calculated by summing the model TOA incoming shortwave (CMIP5 variable "rsdt"), outgoing shortwave (rsut), and outgoing longwave (rlut) radiation fluxes. In order to convert the netTOA flux (i.e., with units watts per square meter) to a heat accumulation/uptake in joules, it was necessary to make use of the CMIP5 atmospheric grid cell area (areacella) variable. Similarly, ocean surface heat uptake (OHU) was calculated using the downward heat flux at sea water surface (hfds) and ocean grid cell area (areacello) variables. For one model, the hfds variable was not archived but could be inferred from the other surface fluxes (Text S1). We define incoming/downward as the positive direction.

2.4. Heat Storage

The CMIP5 variables used to analyze OHC were the sea water potential temperature (thetao) and grid cell volume (volcello). The calculation was performed as follows:

$$\mathrm{OHC}(t, \phi, \lambda) = \rho_0 c_p \sum_z \theta(t, \phi, \lambda, z)\, V(\phi, \lambda, z) \tag{1}$$

where θ is the annually averaged potential temperature at time t, longitude ϕ, latitude λ, and depth z. The reference density is $\rho_0 = 1,023$ kg/m^3, specific heat of water is $c_p = 4,000$ J/(K kg), and the volume of the grid cell $V(\phi, \lambda, z)$. A number of the models had erroneous volcello data (CCSM4, GISS-E2-R, and NorESM-1), so it was calculated using the grid cell area variable (areacello) and the depth intervals from the thetao data.

2.5. Heat Transport

In order to infer meridional heat transports from netTOA, OHU, and OHC data, it was critical that the zonal and hemispheric integration of these quantities conserved the global sum. While such spatial integration is trivial for models run on a regular latitude-longitude grid, more care is needed on curvilinear grids to avoid a nonconservative integral. Similar to a recent study of heat transport into the Arctic Ocean (Nummelin et al., 2017), we make use of the fact that curvilinear CMIP5 data files come with auxiliary coordinate information that specifies the location of each grid point in latitude-longitude space. For zonal integration, we simply added up all grid cells whose auxiliary coordinate fell within each target latitude band. Likewise, hemispheric values were calculated by adding up all grid cells whose auxiliary coordinate fell within a given hemisphere. In this way, we preserved the total fluxes exactly.

In a stationary climate, the long-term mean zonal and hemispheric integrals of netTOA and OHU are not zero at all points (though their global average is). To quantify excess heat uptake, we therefore considered the cumulative sum of the netTOA and OHU anomaly,

$$\sum_{t_0}^{t_x} \mathrm{netTOA}'(t, \lambda) \text{ and } \sum_{t_0}^{t_x} \mathrm{OHU}'(t, \lambda) \tag{2}$$

where t_0 to t_x represents a time period of interest (e.g., 1861–2005) and $'$ indicates an anomaly relative to t_0.

Only two of the models used in this study archived the zonally integrated northward ocean heat transport provided on a regular latitude grid (hfbasin). As such, the accumulated northward ocean heat transport anomaly (OHT') at a given time and latitude was inferred from the cumulative sum (south to north) of the zonally integrated OHU and OHC data:

$$\mathrm{OHT}'(t_x, \lambda_i) = \sum_{-90}^{\lambda_i} \left[\Delta_{t_0}^{t_x} \mathrm{OHC}(\lambda) - \sum_{t_0}^{t_x} \mathrm{OHU}'(t, \lambda) \right] \tag{3}$$

where $\Delta_{t_0}^{t_x}\mathrm{OHC} = \mathrm{OHC}(t_x) - \mathrm{OHC}(t_0)$.

Similarly, the accumulated northward atmospheric heat transport anomaly (AHT') was inferred as follows:

$$\mathrm{AHT}'(t_x, \lambda_i) = \sum_{-90}^{\lambda_i} \left[\sum_{t_0}^{t_x} \mathrm{OHU}'(t, \lambda) - \sum_{t_0}^{t_x} \mathrm{netTOA}'(t, \lambda) \right] \tag{4}$$

For a more detailed overview of the physics behind the climatic energy budget and energy flows (and the fidelity of CMIP5 simulations of these budgets and flows), see Lucarini et al. (2014).

2.6. Drift Removal

Coupled climate models are prone to drift, which refers to spurious long-term trends that are unrelated to changes in external forcing or internal low-frequency variability. It is especially prevalent in model variables linked to the deep ocean, such as those associated with the large-scale uptake, transport, and storage of excess heat. For such variables, drift is typically corrected for by using information from concurrent control experiments (Gupta et al., 2013).

One widely accepted best practice in the drift removal process is to use a drift estimate based on the full control time series, in order to minimize contamination by internal variability. For the various global, hemispheric, and zonal integrals presented in this paper, we obtained a drift estimate by fitting a cubic polynomial to the full control time series (i.e., the integral was calculated first and then dedrifted—the data were not dedrifted prior to calculating the integral). The time period in the control simulation that parallels the forced simulation was then identified using the branch time information provided in the file metadata, so that the correct segment of the cubic polynomial could be subtracted from the forced simulation. For models with erroneous metadata, the branch time was estimated via visual inspection of the globally integrated OHC timeseries (Table S1).

2.7. Model Selection

A basic requirement of any analysis concerning the flow of excess heat through the climate system is closure of the global budget. For annual and longer timescales the ocean represents Earth's primary energy store, and thus, there should be a close correspondence between the globally accumulated netTOA, globally accumulated OHU and the change in global ocean heat storage (i.e., OHC), such that

$$\int_{t_0}^{t_x} \mathrm{netTOA}(t) \approx \int_{t_0}^{t_x} \mathrm{OHU}(t) \approx \Delta_{t_0}^{t_x}\mathrm{OHC} \tag{5}$$

After dedrifting, most CMIP5 models achieve approximate budget closure (Hobbs et al., 2016). Of the six models that performed the experiments and archived the variables of interest in this study, five showed budget closure to within 18%: CanESM2, CCSM4, CSIRO-Mk3-6-0, GISS-E2-R, and NorESM1-M. In other words, for these models the spread in the netTOA, OHU and OHC terms in equation (5) was less than 18% of the average of those terms. Approximate closure was not achieved for the historical experiment of the sixth model (FGOALS-g2) due to an inconsistent netTOA term (Figure S1).

We use the dedrifted data from this five member ensemble for our analysis. Only the first run from each of the five selected models was used, since not all models archived more than one run. (Although the results were not appreciably different when using the mean of each individual model ensemble instead.)

3. The Excess Heat Budget

3.1. Hemispheric Overview

A key feature of the historical experiment was that the global uptake of excess heat at the TOA and ocean surface occurred almost exclusively in the SH (Figure 1). The single forcing experiments show that the uptake associated with GHG forcing was similar for both hemispheres, with AAs canceling that GHG contribution in the NH but having negligible influence in the SH. The largest ensemble spread was at the TOA in the NH, which has been shown to be related to large intermodel differences in aerosol-mediated cloud response (Chung & Soden, 2017).

The oceanic storage of excess heat was also skewed toward the SH in the historical experiment, but in interpreting this result it is necessary to consider that a greater percentage of the global ocean volume resides

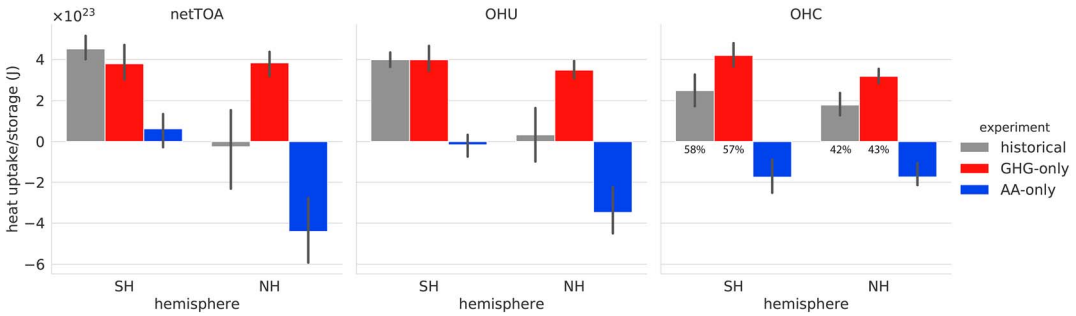

Figure 1. Total hemispheric uptake and storage of excess heat over the period 1861–2005. Ensemble mean values (and the 95% confidence interval) are shown for the accumulated net radiative flux anomaly at the top of the atmosphere (netTOA), accumulated heat flux anomaly at the ocean surface (ocean heat uptake, OHU), and change in ocean heat storage (ocean heat content, OHC). The percentage of global excess heat stored in either hemisphere is indicated for the historical and GHG-only experiments. GHG = greenhouse gas; SH = Southern Hemisphere; NH = Northern Hemisphere.

in the SH (approximately 59%). When this volume effect was removed by considering ocean temperature instead of OHC, the historical experiment showed very little change in temperature difference (NH minus SH) between the hemispheres (Figure 2). In other words, the SH dominance in historical OHU resulted in a compensatory northward ocean heat transport, as opposed to a (volume adjusted) interhemispheric asymmetry in ocean warming. This finding is consistent with the analysis of Lembo et al. (2019), who show that the historical OHC tendency per unit surface area is similar for the two hemispheres.

For most of the twentieth century, the GHG-only experiment also showed little change in hemispheric temperature difference (Figure 2). There was a subtle hint of warming skewed toward the NH in the final decades of the experiment, which is best interpreted in the context of the experiments associated with stronger GHG forcing. For both the 1pctCO2 and RCP 8.5 experiments, the temperature difference between the hemispheres (and thus the oceanic storage of excess heat after accounting for ocean volume) eventually skewed toward the NH. This finding is consistent with simulations of instantaneously quadrupled carbon dioxide, which show a relatively subdued increase in Southern Ocean sea surface temperature in early decades, followed by a strong increase in later decades (Andrews et al., 2015). (Presumably SH heat uptake/storage is less efficient later in the experiment, leading to larger sea surface temperature increases.) While the processes behind ocean heat uptake and storage in state-of-the-art climate models have been studied in detail (e.g., Kuhlbrodt et al., 2015), to the author's knowledge the mechanism behind a possible reduction in the efficiency of Southern Ocean heat uptake/storage with increased GHG forcing (relative to the NH) has not been explored.

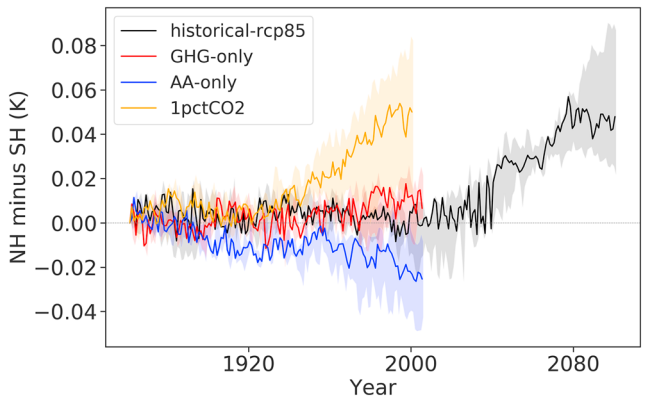

Figure 2. Interhemispheric difference in (volume weighted) average ocean temperature (NH minus SH). The annual mean temperature difference anomaly is shown, where solid lines represent the ensemble median and the shading spans the ensemble interquartile range. SH = Southern Hemisphere; NH = Northern Hemisphere; GHG = greenhouse gas; AA = anthropogenic aerosol.

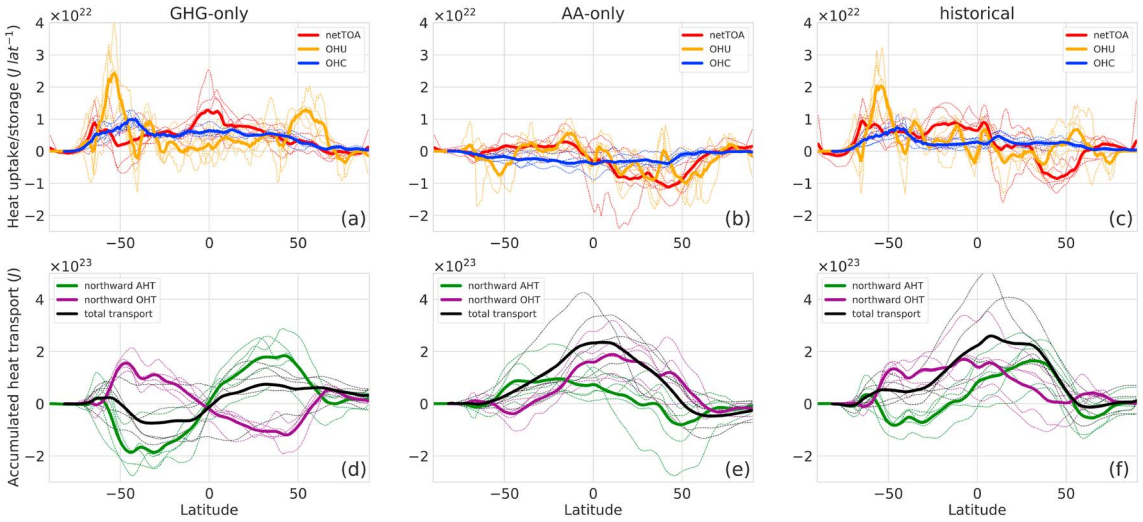

Figure 3. Zonally integrated uptake, transport, and storage of excess heat over the period 1861–2005. Thick lines indicate the ensemble mean, while each of the individual models are shown in thin dashed lines. The top row (a, b, c) shows the accumulated net radiative flux anomaly at the top of the atmosphere (netTOA), accumulated heat flux anomaly at the ocean surface (ocean heat uptake, OHU), and change in ocean heat storage (ocean heat content, OHC), while the bottom row (d, e, f) shows the accumulated northward oceanic heat transport (OHT), atmospheric heat transport (AHT), and total heat transport inferred from those values. GHG = greenhouse gas; AA = anthropogenic aerosol.

To put these temperature changes in context, over the duration of the GHG-only experiment 43% of the globally integrated excess heat was stored in the NH oceans (Figure 1). This percentage increased to 44% over the duration of the 1pctCO2 experiment (Figure S2). In other words, the excess energy budget is qualitatively very similar in the GHG-only and 1pctCO2 experiments (Figure S3), which is why it was necessary to remove the volume effect by looking at temperature in order to identify subtle differences. To demonstrate the robustness of the hemispheric temperature differences from our relatively small ensemble of models, a corresponding analysis of a larger ensemble is shown in Figure S4.

3.2. Meridional Patterns and Transports

3.2.1. GHG-Only Experiment

Net poleward heat transport was enhanced in both hemispheres under GHG forcing (Figure 3d), due to a larger netTOA increase in the tropics and a pattern of ocean heat storage that was comparatively more uniform across latitudes (Figure 3a). Huang and Zhang (2014) show that this pattern of netTOA, as diagnosed in an abrupt quadrupled carbon dioxide experiment, is primarily due to the Planck effect (i.e., emissivity is proportional to temperature). Water vapor feedback also reinforces the equator-to-pole gradient in netTOA, but temperature and albedo feedbacks act against it. The enhanced net poleward heat transport was achieved by a greatly increased poleward atmospheric transport (Figure 3d). This is a robust feature of a warming climate, due to increased atmospheric water vapor content and associated latent heat transport (Held & Soden, 2006).

The increased poleward atmospheric heat transport was partially, but not completely, offset by decreased poleward ocean heat transport in each hemisphere. This result is consistent with a phenomenon known as Bjerknes compensation (Bjerknes, 1964), which states that changes in meridional atmosphere and ocean heat transport will be out-of-phase. While Bjerknes compensation was originally identified and studied in the context of stationary climates (e.g., Shaffrey & Sutton, 2006), it has been shown to operate in transient climate simulations forced by increased atmospheric GHGs (Huang & Zhang, 2014; Outten et al., 2018; Yang et al., 2018). The exact mechanism driving this near compensation in GHG-forced climates is still not clear, although a hint can be gleaned from the meridional OHU pattern. Most of the excess heat enters the ocean in two narrow latitude bands centered around 55°N/S (Figure 3a). Since netTOA is relatively weak at these latitudes but large near the equator, a strong poleward atmospheric transport is required to support this large OHU in the subpolar regions.

In the NH, anomalous ocean heat transport moved heat equatorward from the subpolar zone of maximum OHU, resulting in a slightly greater increase in OHC across the middle-to-low latitudes. This is thought to be related to a slowdown of the Atlantic Meridional Overturning Circulation (AMOC), induced by the

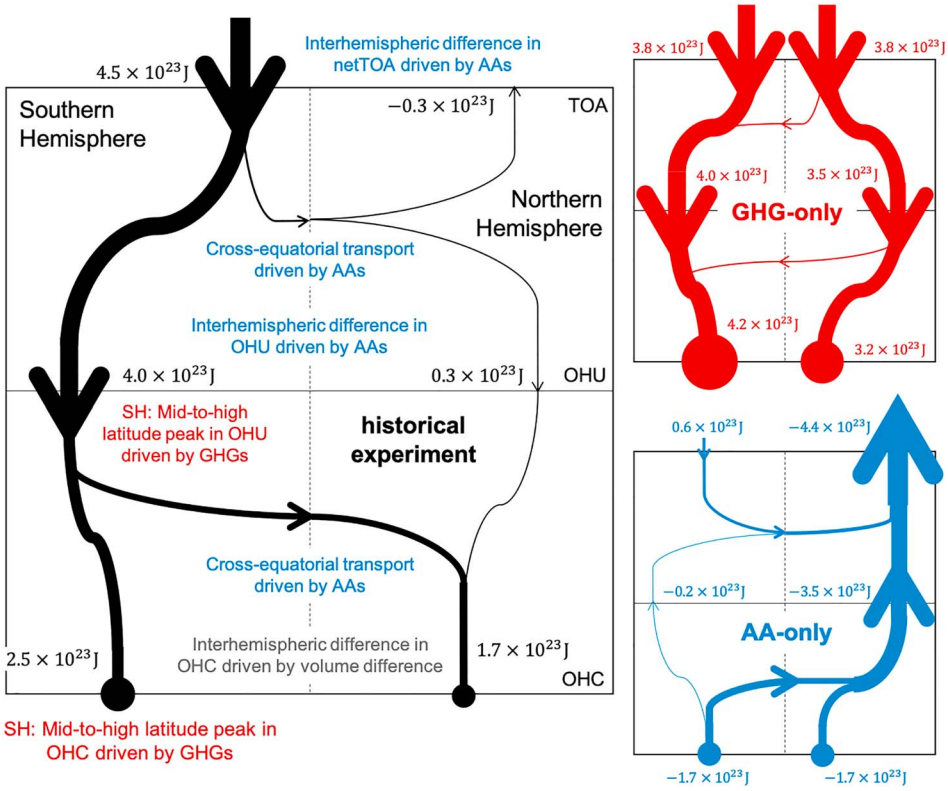

Figure 4. Summary of the drivers of total hemispheric uptake, transport, and storage of excess heat over the period 1861–2005. Ensemble mean values (from Figure 1) are shown for the accumulated net radiative flux anomaly at the top of the atmosphere (netTOA), accumulated heat flux anomaly at the ocean surface (ocean heat uptake, OHU), and change in ocean heat storage (ocean heat content, OHC). The accumulated atmospheric and oceanic heat transport inferred from those values is also indicated, with features of the historical experiment labeled according to whether they are primarily driven by greenhouse gas (GHG) forcing (red text) or anthropogenic aerosol (AA) forcing (blue text).

enhanced OHU and/or freshwater influx at high latitudes (Gregory et al., 2016; Yang et al., 2018). Heat was also transported equatorward from the (larger) OHU maximum centered around 55°S, but with a clear OHC maximum produced near 45°S. This meridional pattern of Southern Ocean warming is thought to be primarily driven by passive advection of the anomalous OHU by the climatological ocean current, with secondary influence from poleward-intensified zonal surface winds (Armour et al., 2016; Liu et al., 2018).

3.2.2. AA-Only Experiment

The classic out-of-phase pattern of excess heat transport associated with Bjerknes compensation was highly modified in the AA-only experiment, as both the atmosphere and ocean transported excess heat northward in response to the large interhemispheric gradients in netTOA and OHU (Figure 3e). It is noteworthy that the bulk of the cross-equatorial transport was performed by the ocean. Previous research has suggested that the ocean does most of the cross-equatorial transport when heat uptake is skewed toward the SH, while the atmosphere dominates when uptake occurs primarily in the NH (McFarlane & Frierson, 2017; White et al., 2018). Our results suggest that the ocean will dominate when heat is preferentially added to the SH (Figure 3f) *or* removed from the NH (Figure 3e).

The AA-only decrease in OHC was relatively uniform across the globe (due to a stronger temperature decline in the smaller NH ocean; Figure 2), except for the absence of any change poleward of 50°N (Figure 3b). This is likely related to the known enhancement of the AMOC in the AA-only experiment, which transports relatively warm waters northward (Shi et al., 2018).

3.2.3. Historical Experiment

The zonally integrated features of the historical experiment can largely be understood as a combination of the GHG and AA responses. As in the AA-only experiment, historical excess heat transport in the atmosphere and ocean deviated significantly from a symmetric Bjerknes compensation pattern, due to the AA-induced SH dominance in heat uptake (Figure 3f). Within the SH, the GHG-forced local maxima in

OHU and OHC were clearly evident in the historical experiment, due to relatively weak (OHU) or absent (OHC) opposition from AA forcing (Figure 3c). In contrast, the GHG-forced peak in OHU in the NH was almost completely canceled by competing AA forcing. The response of the AMOC is known to be approximately equal and opposite in the GHG-only and AA-only experiments (Shi et al., 2018), which means the change in historical OHC was relatively uniform across the NH.

The fact that GHG-only and AA-only excess heat uptake, transport, and storage was approximately linearly additive (i.e., their linear sum closely resembles the historical experiment; Figure S5) suggests that nonlinear effects and other external forcings (e.g., changes in ozone or land use) have negligible influence on a zonally integrated global scale. This is an important result, as it demonstrates that previous studies (e.g., Lembo et al., 2019) were justified in using the difference between the historical and GHG-only experiment to infer the AA influence on energy budget changes. Many other (but not all) climate variables exhibit this additive behavior (Marvel et al., 2015).

3.3. Attribution

Armed with these hemispheric and zonally integrated results from the GHG-only and AA-only experiments (and noting that they are approximately linearly additive), it is possible to nominally attribute various features of the uptake, transport and storage of excess heat over the historical period to GHG or AA forcing (Figure 4). Starting at the TOA, the interhemispheric asymmetry in heat uptake is driven exclusively by AAs. Storage of this excess heat in the ocean is far less asymmetric (it follows the interhemispheric volume distribution), which means AAs are responsible for a northward transport of excess heat in the atmosphere and ocean. Looking at within-hemisphere features, the pronounced uptake of heat at 55°S and related spike in storage at 45°S are clearly attributable to GHG forcing, since AAs have very little influence in the SH. A barrier to formal detection and attribution is often that traditional optimal fingerprinting methods struggle to separate the competing (and approximately symmetrical) influence of GHGs and AAs (Jones et al., 2016). It is promising that so many features relating to the excess energy budget are clearly and solely influenced by AA or GHG forcing.

4. Summary and Discussion

In this study, we take a whole-of-system view in documenting the uptake, transport and storage of excess heat in the climate system. Our analysis of the CMIP5 single forcing experiments indicates that AAs cause the historical uptake of excess heat at the TOA to be strongly skewed toward the SH. This interhemispheric asymmetry in heat uptake is slightly less pronounced at the ocean surface (due to a relatively moderate northward transport of excess heat in the atmosphere), while the oceanic storage of excess heat shows little or no asymmetry after accounting for ocean volume. This requires a relatively large northward transport of excess heat in order to close the oceanic energy budget, which means that simulated changes in historical poleward heat transport deviate significantly from the classic Bjerknes compensation pattern seen in the GHG-only experiment. The interplay between GHG and AA forcing also explains key features within each hemisphere, with AAs offsetting GHG-forced local maxima in OHU in the NH but not the SH.

In many respects, this historical picture is not a good analogue of what can be expected in future. For instance, the projected decline in AA emissions would lead to a much more symmetrical uptake of excess heat between the hemispheres and a consequent reduction in the northward transport of excess heat (e.g., Figure S6). Our results also suggest that GHG forcing stronger than that experienced over the historical period (i.e., the GHG forcing projected for coming decades) is associated with an oceanic storage of excess heat skewed toward the NH (after accounting for ocean volume). The mechanisms behind this result represent an interesting avenue for future research. In particular, is it possible to identify the SH/Southern Ocean processes that make it less efficient (relative to the NH/North Atlantic) at storing excess heat as GHG concentrations rise?

Further research is also needed to formally attribute specific climate impacts and circulation responses to AA- or GHG-induced uptake, transport and/or storage of excess heat. So far the progress on this front has focused on the atmosphere, where northward heat transport associated with AA forcing has been linked with an observed southward shift of the Intertropical Convergence Zone and associated drought in the African Sahel region (Hwang et al., 2013). The single forcing experiments conducted as part of CMIP6 (Gillett et al., 2016) will extend to 2020 and thus overlap with the Argo era, possibly providing new opportunities for similar ocean-based studies.

Acknowledgments
We acknowledge the World Climate Research Programme's Working Group on Coupled Modelling, which is responsible for CMIP, and we thank the climate modeling groups for producing and making available their model output. CMIP data can be accessed at the ESGF website (https://esgfnode.llnl.gov/projects/esgfllnl/). For CMIP the U.S. Department of Energy's Program for Climate Model Diagnosis and Intercomparison provides coordinating support and led development of software infrastructure in partnership with the Global Organization for Earth System Science Portals. We also thank Paola Petrelli from the ARC Centre of Excellence for Climate Extremes, for her assistance with downloading/managing the CMIP5 data archive at the National Computational Infrastructure.

References

Andrews, T., Gregory, J. M., & Webb, M. J. (2015). The dependence of radiative forcing and feedback on evolving patterns of surface temperature change in climate models. *Journal of Climate*, *28*, 1630–1648. https://doi.org/10.1175/JCLI-D-14-00545.1

Armour, K. C., Marshall, J., Scott, J. R., Donohoe, A., & Newsom, E. R. (2016). Southern Ocean warming delayed by circumpolar upwelling and equatorward transport. *Nature Geoscience*, *9*, 549–554. https://doi.org/10.1038/ngeo2731

Bjerknes, J. (1964). Atlantic air-sea interaction. *Advances in Geophysics*, *10*, 1–82. https://doi.org/10.1016/S0065-2687(08)60005-9

Boucher, O., Randall, D., Artaxo, P., Bretherton, C., Feingold, G., Forster, P., et al. (2013). Clouds and Aerosols. In T. Stocker (Ed.), *Climate Change 2013: The Physical Science Basis. Contribution of Working Group I to the Fifth Assessment Report of the Intergovernmental Panel on Climate Change* (pp. 571–657). Cambridge, United Kingdom and New York, NY, USA: Cambridge University Press.

Chung, E.-S., & Soden, B. J. (2017). Hemispheric climate shifts driven by anthropogenic aerosol-cloud interactions. *Nature Geoscience*, *10*, 566–571. https://doi.org/10.1038/ngeo2988

Gillett, N. P., Shiogama, H., Funke, B., Hegerl, G., Knutti, R., Matthes, K., et al. (2016). The Detection and Attribution Model Intercomparison Project (DAMIP v1.0) contribution to CMIP6. *Geoscientific Model Development*, *9*, 3685–3697. https://doi.org/10.5194/gmd-9-3685-2016

Gregory, J. M., Bouttes, N., Griffies, S. M., Haak, H., Hurlin, W. J., Jungclaus, J., et al. (2016). The Flux-Anomaly-Forced Model Intercomparison Project (FAFMIP) contribution to CMIP6: Investigation of sea-level and ocean climate change in response to CO2 forcing. *Geoscientific Model Development*, *9*, 3993–4017. https://doi.org/10.5194/gmd-9-3993-2016

Gupta, A. S., Jourdain, N. C., Brown, J. N., & Monselesan, D. (2013). Climate drift in the CMIP5 models. *Journal of Climate*, *26*, 8597–8615. https://doi.org/10.1175/JCLI-D-12-00521.1

Held, I. M., & Soden, B. J. (2006). Robust responses of the hydrological cycle to global warming. *Journal of Climate*, *19*, 5686–5699. https://doi.org/10.1175/JCLI3990.1

Hobbs, W., Palmer, M. D., & Monselesan, D. (2016). An energy conservation analysis of ocean drift in the CMIP5 global coupled models. *Journal of Climate*, *29*, 1639–1653. https://doi.org/10.1175/JCLI-D-15-0477.1

Huang, Y., & Zhang, M. (2014). The implication of radiative forcing and feedback for meridional energy transport. *Geophysical Research Letters*, *41*, 1665–1672. https://doi.org/10.1002/2013GL059079

Hunter, J. D. (2007). Matplotlib: A 2D graphics environment. *Computing in Science and Engineering*, *9*, 99–104. https://doi.org/10.1109/MCSE.2007.55

Hwang, Y.-T., Frierson, D. M. W., & Kang, S. M. (2013). Anthropogenic sulfate aerosol and the southward shift of tropical precipitation in the late 20th century. *Geophysical Research Letters*, *40*, 2845–2850. https://doi.org/10.1002/grl.50502

Irving, D. B. (2016). A minimum standard for publishing computational results in the weather and climate sciences. *Bulletin of the American Meteorological Society*, *97*, 1149–1158. https://doi.org/10.1175/BAMS-D-15-00010.1

Irving, D. B. (2019). Anthropogenic aerosols, greenhouse gases and the uptake, transport and storage of excess heat in the climate system: Supplementary metadata, Figshare. Retrieved from https://doi.org/10.6084/m9.figshare.7575830.v3

Jones, G. S., Stott, P. A., & Mitchell, J. F. B. (2016). Uncertainties in the attribution of greenhouse gas warming and implications for climate prediction. *Journal of Geophysical Research: Atmospheres*, *121*, 6969–6992. https://doi.org/10.1002/2015JD024337

Kuhlbrodt, T., Gregory, J. M., & Shaffrey, L. C. (2015). A process-based analysis of ocean heat uptake in an AOGCM with an eddy-permitting ocean component. *Climate Dynamics*, *45*, 3205–3226. https://doi.org/10.1007/s00382-015-2534-0

Lembo, V., Folini, D., Wild, M., & Lionello, P. (2019). Inter-hemispheric differences in energy budgets and cross-equatorial transport anomalies during the 20th century. *Climate Dynamics*. https://doi.org/10.1007/s00382-018-4572-x

Liu, W., Lu, J., Xie, S.-P., & Fedorov, A. (2018). Southern Ocean heat uptake, redistribution, and storage in a warming climate: The role of meridional overturning circulation. *Journal of Climate*, *31*, 4727–4743. https://doi.org/10.1175/JCLI-D-17-0761.1

Lucarini, V., Blender, R., Herbert, C., Ragone, F., Pascale, S., & Wouters, J. (2014). Mathematical and physical ideas for climate science. *Reviews of Geophysics*, *52*, 809–859. https://doi.org/10.1002/2013RG000446

Marvel, K., Schmidt, G. A., Shindell, D., Bonfils, C., LeGrande, A. N., Nazarenko, L., & Tsigaridis, K. (2015). Do responses to different anthropogenic forcings add linearly in climate models? *Environmental Research Letters*, *10*, 104010. https://doi.org/10.1088/1748-9326/10/10/104010

McFarlane, A. A., & Frierson, D. M. W. (2017). The role of ocean fluxes and radiative forcings in determining tropical rainfall shifts in RCP8.5 simulations. *Geophysical Research Letters*, *44*, 8656–8664. https://doi.org/10.1002/2017GL074473

Met Office (2010–2018). Iris: A Python library for analysing and visualising meteorological and oceanographic data sets (v2.0 ed.) [Computer software manual]. Exeter, Devon. Retrieved from http://scitools.org.uk/

Nummelin, A., Li, C., & Hezel, P. J. (2017). Connecting ocean heat transport changes from the midlatitudes to the Arctic Ocean. *Geophysical Research Letters*, *44*, 1899–1908. https://doi.org/10.1002/2016GL071333

Outten, S., Esau, I., & Otterå, O. H. (2018). Bjerknes compensation in the CMIP5 climate models. *Journal of Climate*, *31*, 8745–8760. https://doi.org/10.1175/JCLI-D-18-0058.1

Roelofs, G.-J. (2013). A steady-state analysis of the temperature responses of water vapor and aerosol lifetimes. *Atmospheric Chemistry and Physics*, *13*, 8245–8254. https://doi.org/10.5194/acp-13-8245-2013

Shaffrey, L., & Sutton, R. (2006). Bjerknes compensation and the decadal variability of the energy transports in a coupled climate model. *Journal of Climate*, *19*, 1167–1181. https://doi.org/10.1175/JCLI3652.1

Shi, J.-R., Xie, S.-P., & Talley, L. D. (2018). Evolving relative importance of the Southern Ocean and North Atlantic in anthropogenic ocean heat uptake. *Journal of Climate*, *31*, 7459–7479. https://doi.org/10.1175/JCLI-D-18-0170.1

Smith, S. J., Rao, S., Riahi, K., van Vuuren, D. P., Calvin, K. V., & Kyle, P. (2016). Future aerosol emissions: A multi-model comparison. *Climatic Change*, *138*, 13–24. https://doi.org/10.1007/s10584-016-1733-y

Taylor, K. E., Stouffer, R. J., & Meehl, G. A. (2012). An overview of CMIP5 and the experiment design. *Bulletin of the American Meteorological Society*, *93*, 485–498. https://doi.org/10.1175/BAMS-D-11-00094.1

Van Der Walt, S., Colbert, S. C., & Varoquaux, G. (2011). The NumPy array: A structure for efficient numerical computation. *Computing in Science and Engineering*, *13*, 22–30. https://doi.org/10.1109/MCSE.2011.37

van Vuuren, D. P., Edmonds, J., Kainuma, M., Riahi, K., Thomson, A., Hibbard, K., et al. (2011). The Representative Concentration Pathways: An overview. *Climatic Change*, *109*, 5–31. https://doi.org/10.1007/s10584-011-0148-z

von Schuckmann, K., Palmer, M. D., Trenberth, K. E., Cazenave, A., Chambers, D., Champollion, N., et al. (2016). An imperative to monitor Earth's energy imbalance. *Nature Climate Change*, *6*, 138–144. https://doi.org/10.1038/nclimate2876

Wang, H., Xie, S.-P., & Liu, Q. (2016). Comparison of climate response to anthropogenic aerosol versus greenhouse gas forcing: distinct patterns. *Journal of Climate*, *29*, 5175–5188. https://doi.org/10.1175/JCLI-D-16-0106.1

Waskom, M. (2018). Seaborn: statistical data visualization (v0.9.0) [Computer software manual]. http://seaborn.pydata.org, https://doi.org/10.5281/zenodo.1313201

White, R. H., McFarlane, A. A., Frierson, D. M. W., Kang, S. M., Shin, Y., & Friedman, M. (2018). Tropical precipitation and cross-equatorial heat transport in response to localized heating: basin and hemisphere dependence. *Geophysical Research Letters*, *45*, 11949–11958. https://doi.org/10.1029/2018GL078781

Xie, S.-P., Lu, B., & Xiang, B. (2013). Similar spatial patterns of climate responses to aerosol and greenhouse gas changes. *Nature Geoscience*, *6*, 828–832. https://doi.org/10.1038/ngeo1931

Yang, Q., Zhao, Y., Wen, Q., Yao, J., & Yang, H. (2018). Understanding Bjerknes compensation in meridional heat transports and the role of freshwater in a warming climate. *Journal of Climate*, *31*, 4791–4806. https://doi.org/10.1175/JCLI-D-17-0587.1